Check for updates

A continuum model based on Rayleigh dissipation functions to describe a Coulomb-type constitutive law for internal friction in woven fabrics

Alessandro Ciallella, Daria Scerrato, Mario Spagnuolo and Ivan Giorgio

Abstract. A continuum model intended to provide predictions for the response of a woven fabric that includes the effects of friction between fibers is proposed. Specifically, we consider a macroscopic formulation in which the fabric weave is composed of two orthogonal families of continuously distributed yarns. The elastic behavior of the planar fabric is characterized by a second-gradient formulation, incorporating the capacity of the fibers to resist a bending deformation. Particular care is devoted to modeling the action of preventing fiber overlapping through a potential energy barrier. The frictional sliding effect of warp threads interwoven with the weft yarns is introduced through a Rayleigh dissipative function that can be appropriately shaped to consider a Coulomb-type law. Spinning friction of yarns belonging to different families also is conceived when a relative rotation between fibers is present to generalize the dissipation phenomenon involved in the considered sheet. Numerical simulations of the proposed model are provided and discussed.

1. Introduction

Recent developments in continuum mechanics are increasingly marked by the need to model the mechanical phenomenology occurring in "complex" metamaterials [21,22]. These are materials designed for getting a specific << a priori-chosen>> behavior by finding suitable micro-architectures (see, e.g., [1,2,32,51,55,58,65–67]). In this context, the synthesis problem of metamaterials governed by a chosen set of evolution equations plays a crucial role (see, e.g., [4,9,14,24,30,47,48,60]). When trying to synthesize the "second gradient" continua, the particular micro-architecture that has been called "pantographic" seems to play an important role. In fact, such micro-architecture allows for, at the macro-level, large elongations and (with specific micro-constraints) more generally macro-deformations that correspond to low deformation energies [3,17,19,41,42,50].

In the papers [5,6,8,10], it has been proven that by combining pantographic beams [7,38,61–63] via suitable mechanical interconnections, a more general second gradient planar plates can be synthesized. Some endeavors are being done in order to synthesize 3D continua whose deformation energy depends on all second-order derivatives of displacement [26,59,68].

Pantographic micro-structure was inspired by the study of composite fibers reinforcements, whose mechanical behavior has been puzzling many scholars because of their peculiarities (see, e.g., [13,29,35, 39,40]).

The concept behind pantographic micro-structures assumes that fibers belonging to different families are allowed to have relative displacements and relative rotations (at the micro-level) and that these displacements and rotations are possible with a vanishing or minimal deformation energy. This concept is not entirely new, as it has been exploited in several technological circumstances, particularly in the woven fabrics used as reinforcements in composites. The possibility of these relative displacements and

rotations also in pantographic micro-architectures did motivate the formulation of continuum models in which enriched kinematics is introduced. For instance, in [56,57], two kinematical fields are introduced to describe the placement of each of the two families of fibers constituting the micro-architecture.

Instead, in [37], the kinematics is even richer, as two rotation fields are added. These more detailed kinematical descriptions are strongly motivated by the need to describe experimental evidence and the request to use a "computationally manageable" reduced-order model. In fact, at least in principle, the experimental evidence could have been described by introducing a very detailed 3D Cauchy first gradient continuum modeling the microstructure at the length scale of the constituting fibers' diameter, but the computational burden would have been several millions of degrees of freedom. Such a burden, especially when optimization problems need to be solved [23,33,34], would make any analysis almost unattainable.

In the present paper, we formulate a continuum model designed to give a reduced-order description for the response of a woven fabric whose mechanical behavior has some similarities with that of pantographic sheets. The described phenomenology includes the effects of slipping friction and those involved in the contact among fibers. Refraining, for the moment, from any detailed microscopic analysis, we propose directly a macroscopic model aiming to account for the deformation of a fabric whose weave is composed of two orthogonal families of homogeneously distributed yarns. The imagined planar fabric has a complex mechanical behavior: its elasticity properties will be mathematically modeled by introducing a second gradient deformation energy, which will account for the capacity of the fibers to resist bending deformations. Moreover, the interaction between fibers in contact is also assumed to be elastic with an interaction potential that tends quickly to infinity to block possible fibers' interpenetrations. Additional dissipative effects are incorporated in the model in order to account for: (1) the frictional sliding effect of warp threads interwoven with the weft yarns and (2) spinning friction of yarns belonging to different fibers families. The modeling choice consists in introducing a suitable Rayleigh dissipative function. Such a function is chosen to produce a Coulomb-type friction law among fibers. Spinning friction is introduced in order to model those dissipative phenomena occurring when a relative rotation between fibers is present and plays a relevant role in considered deformation phenomena. More generally, modeling internal dissipation in solids is an age-old problem, and for this reason, a huge amount of literature concerning this subject is available (see [11,12,54,64] for helpful insight on the topic). In these contributions, the dissipated energy often participates in damage and plastic phenomena—possibly by producing cracks or enlarging the existing ones. On the other hand, the dissipated energy could also be associated with friction related to reversible internal relative motions. This last aspect is often underestimated or taken into account through some viscous effects that do not fit the experimental responses of the material since it introduces a rate-dependent behavior not present. Only a few studies are available in this regard in the literature about internal Coulomb-type dissipation in solids [36,52] and more specifically in woven fabrics (see, e.g., [31,43]).

The discussed problem is closely related to the adhesion of thin films and fibers [25,44]; therefore, we believe that the applications of the proposed model can also be extended to these kinds of problems.

The proposed model is validated by performing numerical simulations, which produce interesting predictions about the mechanical behavior of the considered fabric. It has to be remarked that the presented methods may be of use also in the design of pantographic metamaterials: in fact, the considered frictional phenomenology has not been studied yet in this last context apart from one preliminary attempt done in [15].

2. Modeling

To model a woven fabric, a continuum elastic surface $\mathcal{S}$, lying on a rectangular region Ω belonging to a bi-dimensional Euclidean space, is regarded as a double family of straight orthogonal fibers, i.e., the yarns in warp and weft directions, continuously distributed. More precisely, for the plane surface $\mathcal{S}$ and

at a given time, a motion, herein regarded as planar, is defined by two placement vector fields, denoted by $\boldsymbol{\chi}_1$ and $\boldsymbol{\chi}_2$, for the two families of fibers.

A practical choice for this kind of engineering fabric is to represent all deformation measures in a reference frame aligned with the fiber directions. For this purpose, the unit tangent vectors to the two families of fibers in the reference configuration, denoted by $\mathbf{D}_1$ and $\mathbf{D}_2$, are introduced. Consequently, to model the elastic behavior of the textile formed by weaving fibers, all elastic constitutive information is represented through a strain energy

$$\mathscr{W}\left(\boldsymbol{\chi}_2 - \boldsymbol{\chi}_1, \nabla\boldsymbol{\chi}_1, \nabla\boldsymbol{\chi}_2, \nabla\nabla\boldsymbol{\chi}_1, \nabla\nabla\boldsymbol{\chi}_2\right) \tag{1}$$

that depends on the relative fiber displacement, the first, and second gradients of the placement. A strain-energy function of this type [18,56], incorporating the orthotropic response conferred by the initial fiber geometry, is

$$\mathscr{W} = \int_\Omega \sum_\alpha \frac{\mathscr{K}_e^\alpha}{2}(\|\nabla\boldsymbol{\chi}_\alpha\mathbf{D}_\alpha\| - 1)^2 \, \mathrm{d}\Omega + \int_\Omega \frac{\mathscr{K}_s}{2}\left[\tan\left(\arcsin\left(\frac{\nabla\boldsymbol{\chi}_1\mathbf{D}_1}{\|\nabla\boldsymbol{\chi}_1\mathbf{D}_1\|} \cdot \frac{\nabla\boldsymbol{\chi}_2\mathbf{D}_2}{\|\nabla\boldsymbol{\chi}_2\mathbf{D}_2\|}\right)\right)\right]^2 \, \mathrm{d}\Omega$$

$$+ \int_\Omega \sum_\alpha \frac{\mathscr{K}_b^\alpha}{2}\left[\frac{\nabla\nabla\boldsymbol{\chi}_\alpha\mathbf{D}_\alpha\,|\mathbf{D}_\alpha\otimes\mathbf{D}_\alpha \cdot \nabla\nabla\boldsymbol{\chi}_\alpha\mathbf{D}_\alpha\,|\mathbf{D}_\alpha\otimes\mathbf{D}_\alpha}{\|\nabla\boldsymbol{\chi}_\alpha\mathbf{D}_\alpha\|^2}\right.$$

$$\left. - \left(\frac{\nabla\boldsymbol{\chi}_\alpha\mathbf{D}_\alpha}{\|\nabla\boldsymbol{\chi}_\alpha\mathbf{D}_\alpha\|} \cdot \frac{\nabla\nabla\boldsymbol{\chi}_\alpha\mathbf{D}_\alpha\,|\mathbf{D}_\alpha\otimes\mathbf{D}_\alpha}{\|\nabla\boldsymbol{\chi}_\alpha\mathbf{D}_\alpha\|}\right)^2\right] \, \mathrm{d}\Omega + \int_\Omega \frac{\mathscr{K}_c}{2}\|\boldsymbol{\chi}_2 - \boldsymbol{\chi}_1\|^2 \, \mathrm{d}\Omega \tag{2}$$

in which $\mathscr{K}_e^\alpha$, $\mathscr{K}_s$ and $\mathscr{K}_b^\alpha$ are material parameters related to the extensional, shear, and bending stiffness, respectively, being $\alpha = \{1, 2\}$ a label that specifies one of the two families of the fibers. The stiffness $\mathscr{K}_c$ concerns the elastic interaction between fibers belonging to different families. Specifically, the measures of deformation appearing in the stored strain energy are:

1. the *stretching of fibers*

$$\varepsilon_\alpha = \|\nabla\boldsymbol{\chi}_\alpha\mathbf{D}_\alpha\| - 1\,; \tag{3}$$

2. the *shearing distortion*:

$$\gamma = \arcsin\left(\frac{\nabla\boldsymbol{\chi}_1\mathbf{D}_1}{\|\nabla\boldsymbol{\chi}_1\mathbf{D}_1\|} \cdot \frac{\nabla\boldsymbol{\chi}_2\mathbf{D}_2}{\|\nabla\boldsymbol{\chi}_2\mathbf{D}_2\|}\right) \tag{4}$$

   namely the change in the angle between fibers belonging to different families;

3. the *Lagrangian curvature of fibers*:

$$\kappa_\alpha = \sqrt{\frac{\nabla\nabla\boldsymbol{\chi}_\alpha\mathbf{D}_\alpha\,|\mathbf{D}_\alpha\otimes\mathbf{D}_\alpha \cdot \nabla\nabla\boldsymbol{\chi}_\alpha\mathbf{D}_\alpha\,|\mathbf{D}_\alpha\otimes\mathbf{D}_\alpha}{\|\nabla\boldsymbol{\chi}_\alpha\mathbf{D}_\alpha\|^2} - \left(\frac{\nabla\boldsymbol{\chi}_\alpha\mathbf{D}_\alpha}{\|\nabla\boldsymbol{\chi}_\alpha\mathbf{D}_\alpha\|} \cdot \frac{\nabla\nabla\boldsymbol{\chi}_\alpha\mathbf{D}_\alpha\,|\mathbf{D}_\alpha\otimes\mathbf{D}_\alpha}{\|\nabla\boldsymbol{\chi}_\alpha\mathbf{D}_\alpha\|}\right)^2} \tag{5}$$

   that is the rate of change of the current tangent vector to the fiber with respect to arc length along the same fiber in the reference configuration;

4. the *coupling distortion*

$$\beta = \|\boldsymbol{\chi}_2 - \boldsymbol{\chi}_1\| \tag{6}$$

   which represents the interaction term between the two families of fibers. This interaction is due to the geometry of the contact between fibers. The mechanism characterizing such an interaction is analogous to a leaf spring (see Fig. 1).

It is worth noting that the energy density related to the shear deformation is written in terms of the tangent of the distortion angle γ [49]; this is a natural way of excluding the overlapping of the fibers since the trigonometric function tends only asymptotically to the values $\pm\pi/2$ for which it would be necessary to provide an infinite amount of energy to the sample.
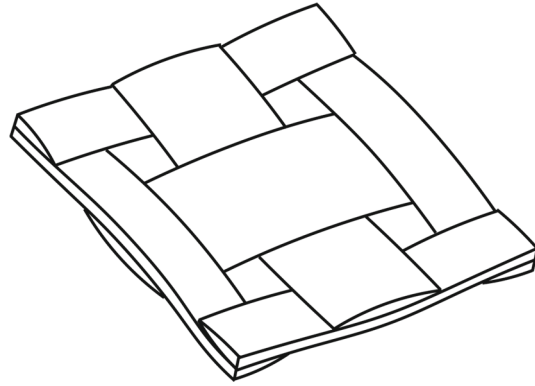
Fig. 1. Unit cell of the woven fabric

Table 1. *Material parameters used in the numerical simulations*

parameter	value
$\mathscr{K}_e^\alpha$	1.27×10^8 N/m
$\mathscr{K}^s$	4.00×10^2 N/m
$\mathscr{K}_b^\alpha$	254.1 N m
$\mathscr{K}_c$	6.00×10^7 N/m^3
ζ	199.2 kN/m^2
η	70 s/m

2.1. Model of dissipation

In the present work, the effects of slipping with friction are considered by means of a macroscopic formulation based on the choice of a suitable dissipation functional which depends on the relative sliding velocities between the two interacting families of fibers [20]. For this purpose, a Rayleigh dissipative potential density is introduced as follows:

$$\mathscr{R} = \frac{\zeta}{\eta} \left\{ \log\left[\cosh\left(\eta\left(\dot{\chi}_{11} - \dot{\chi}_{21}\right)\right)\right] + \log\left[\cosh\left(\eta\left(\dot{\chi}_{12} - \dot{\chi}_{22}\right)\right)\right] \right\} \tag{7}$$

to model a Coulomb-type friction dissipation and is designed by means of the components of the relative velocity $\dot{\boldsymbol{\chi}}_1 - \dot{\boldsymbol{\chi}}_2$. Following this approach, the derivative of such a potential density $\mathscr{R}$ with respect to the relative sliding velocities in the directions $\mathbf{D}_1$ and $\mathbf{D}_2$ yields the friction stress $\boldsymbol{\tau}$ mutually exerted by the fibers during a sliding motion, whose components are:

$$\tau_i = \zeta \tanh\left[\eta\left(\dot{\chi}_{1i} - \dot{\chi}_{2i}\right)\right] \tag{8}$$

In the literature, Coulomb friction actions are usually modeled by the introduction of the *signum* function, whose argument is the velocity of the kinematical quantity on which friction forces act. This function, being not Lipschitz continuous, is a source of strong singularities and numerical or chaotic instabilities when appearing in differential equations. Therefore, the *signum* function is regularized with a hyperbolic tangent modulated with an amplitude ζ—giving the maximum of friction stress which may be exerted—and with a suitably chosen slope given by η —defining the range of velocities where a viscous behavior is present, namely the friction force is an increasing function of the velocity.
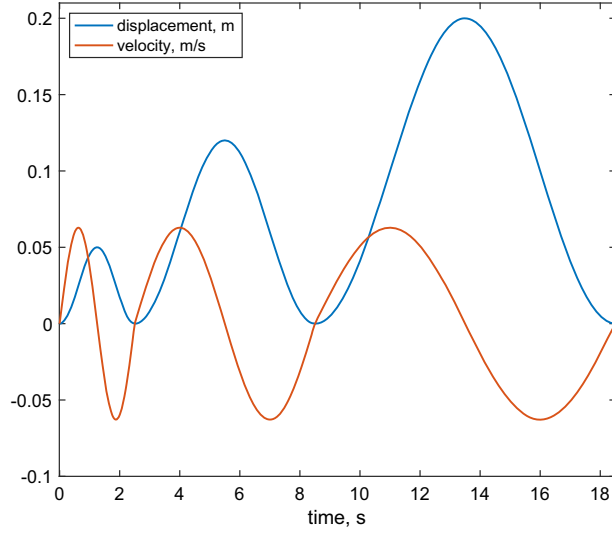
FIG. 2. Plots of the applied displacement and velocity in the cyclic tensile tests. Case of constant maximum velocity
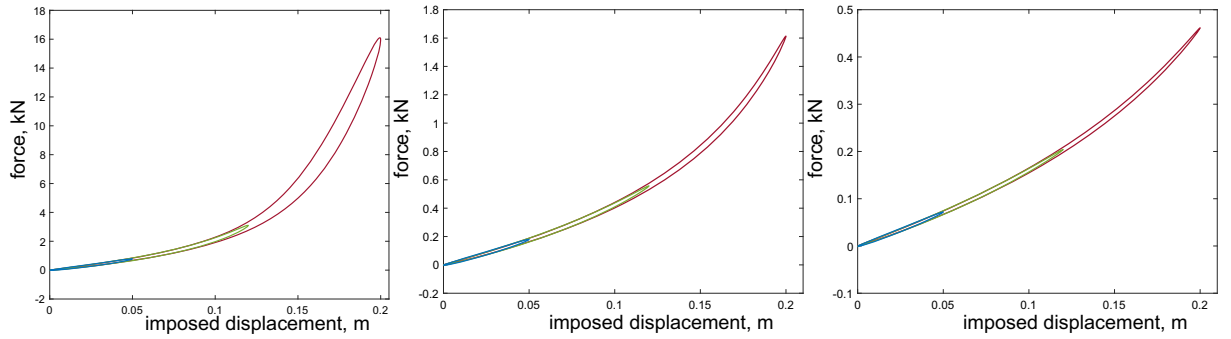

FIG. 3. Hysteretic cycles for different aspect ratios: 1:2 (left); 1:3 (center); 1:4 (right)

Therefore, the virtual work related to the friction has to be calculated as follows:

$$\delta \mathscr{W}^{\mathrm{Diss}} = - \int_{\Omega} \boldsymbol{\tau} \cdot \delta \left(\boldsymbol{\chi}_1 - \boldsymbol{\chi}_2 \right) \mathrm{d}\Omega \tag{9}$$

2.2. Spinning friction

Since the nature of the contact is particularly complex in the considered system, in the present paper, we also explore the possibility of adding a dissipation related to the relative rotation of the fibers that are into contact. Indeed, it is reasonably expected that a relative rotation of the small regions belonging to different fibers in touch produces a share of dissipation in the overall motion due to this kind of contact that is not provided by the model given in (9). For this purpose, a spinning friction term [69] is conceived through a Rayleigh dissipative potential as a function of the relative rotation rate $\dot{\gamma}$:
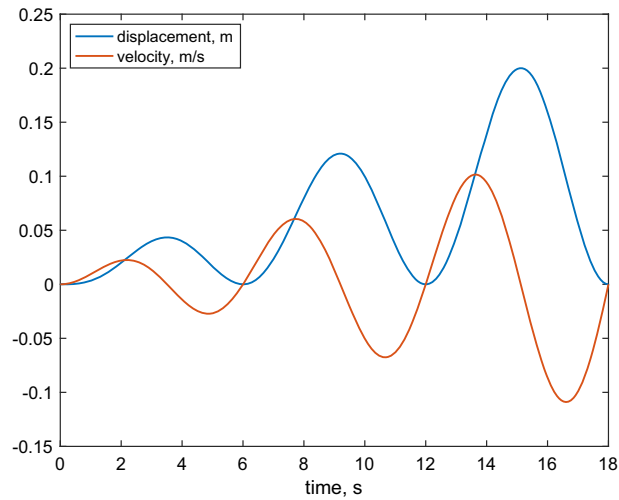
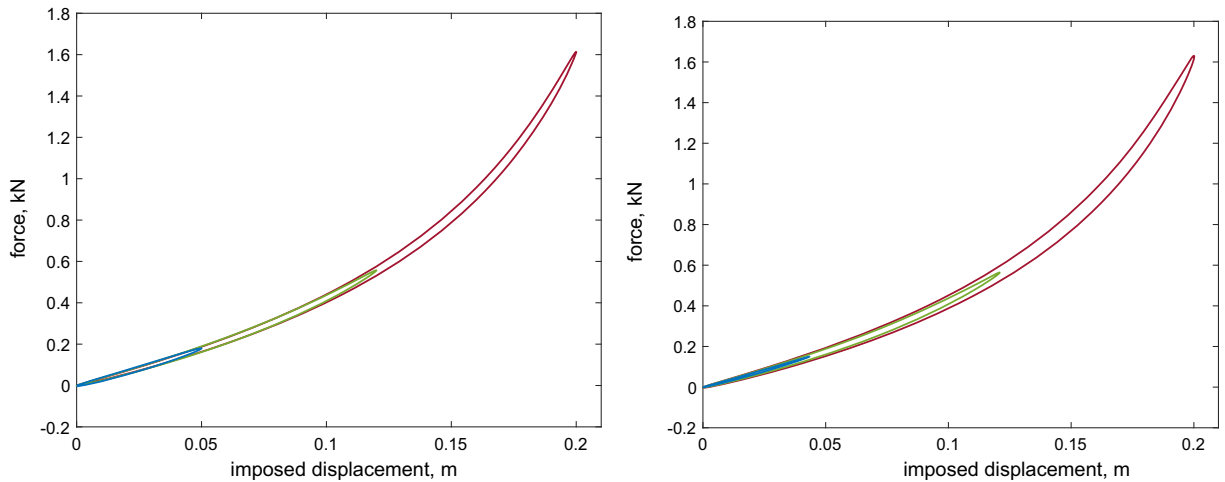FIG. 4. Plots of the applied displacement and velocity in the cyclic tensile tests. Case of constant frequency

FIG. 5. Comparison between the hysteretic cycles for the sample with ratio 1:3 for the constant maximum velocity case (left) and the constant frequency case (right)

$$\mathscr{R}_{\mathrm{spin}} = \frac{\zeta_{\mathrm{spin}}}{\eta_{\mathrm{spin}}} \log\left[\cosh\left(\eta_{\mathrm{spin}}\dot{\gamma}\right)\right] \tag{10}$$

in which ζ_{spin} and η_{spin} play an analogous role of the previous sliding friction contribution. Therefore, the virtual work related to the spinning friction becomes

$$\delta\mathscr{W}_{\mathrm{spin}}^{\mathrm{Diss}} = -\int_{\Omega} \zeta_{\mathrm{spin}} \tanh\left(\eta_{\mathrm{spin}}\dot{\gamma}\right) \delta\gamma \, \mathrm{d}\Omega\,. \tag{11}$$

Finally, considering the case in which inertial effects can be neglected and to get the equations of motion, the first variation of the strain-energy functional $\mathscr{W}$ has to be equated to the dissipative virtual works, i.e.,
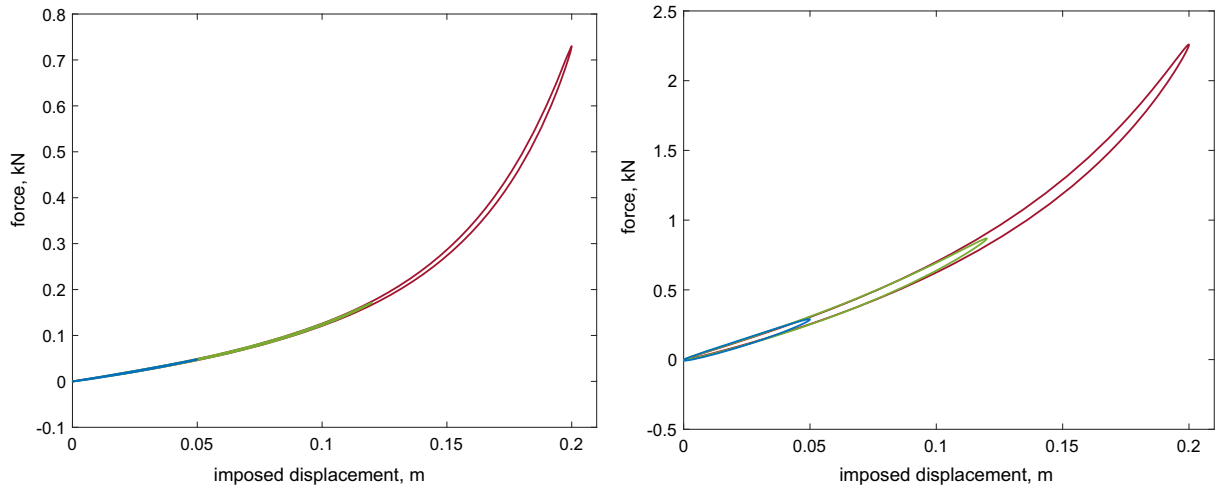
FIG. 6. Comparison between the hysteretic cycles for the sample with ratio 1:3 for a soft bending stiffness case (left) and a hard bending stiffness case (right)
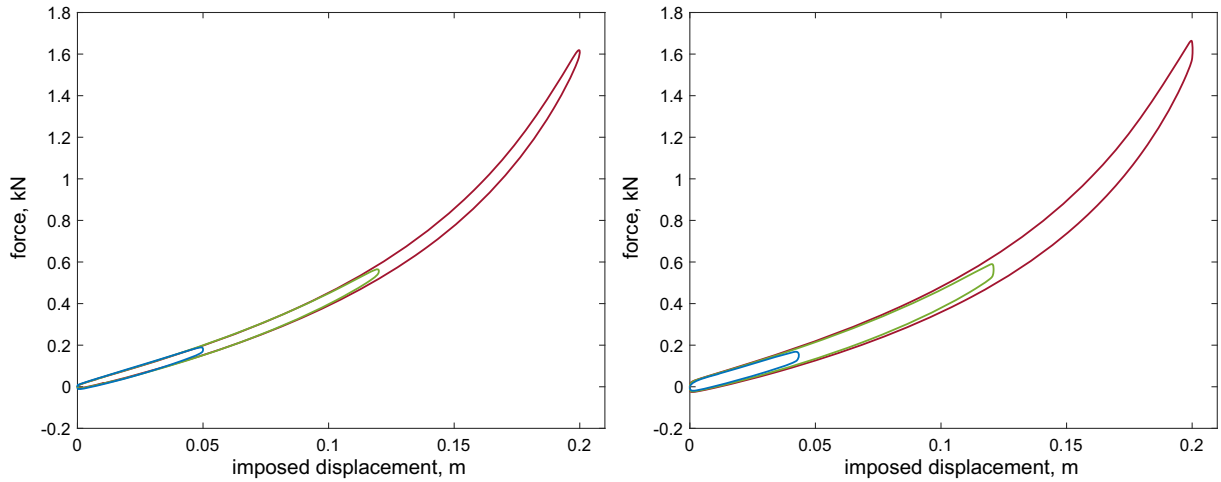

FIG. 7. Comparison between the hysteretic cycles with spinning friction for the sample with ratio 1:3 for the constant maximum velocity case (left) and the constant frequency case (right)

$$\delta \mathscr{W} = \delta \mathscr{W}^{\mathrm{Diss}} + \delta \mathscr{W}^{\mathrm{Diss}}_{\mathrm{spin}} . \tag{12}$$

possibly, at first approximation, the last term can be neglected. In what follows, for the sake of simplicity, we consider only kinematic boundary conditions on a portion of the boundary while other parts are free. Therefore, no external work is taken into account here.
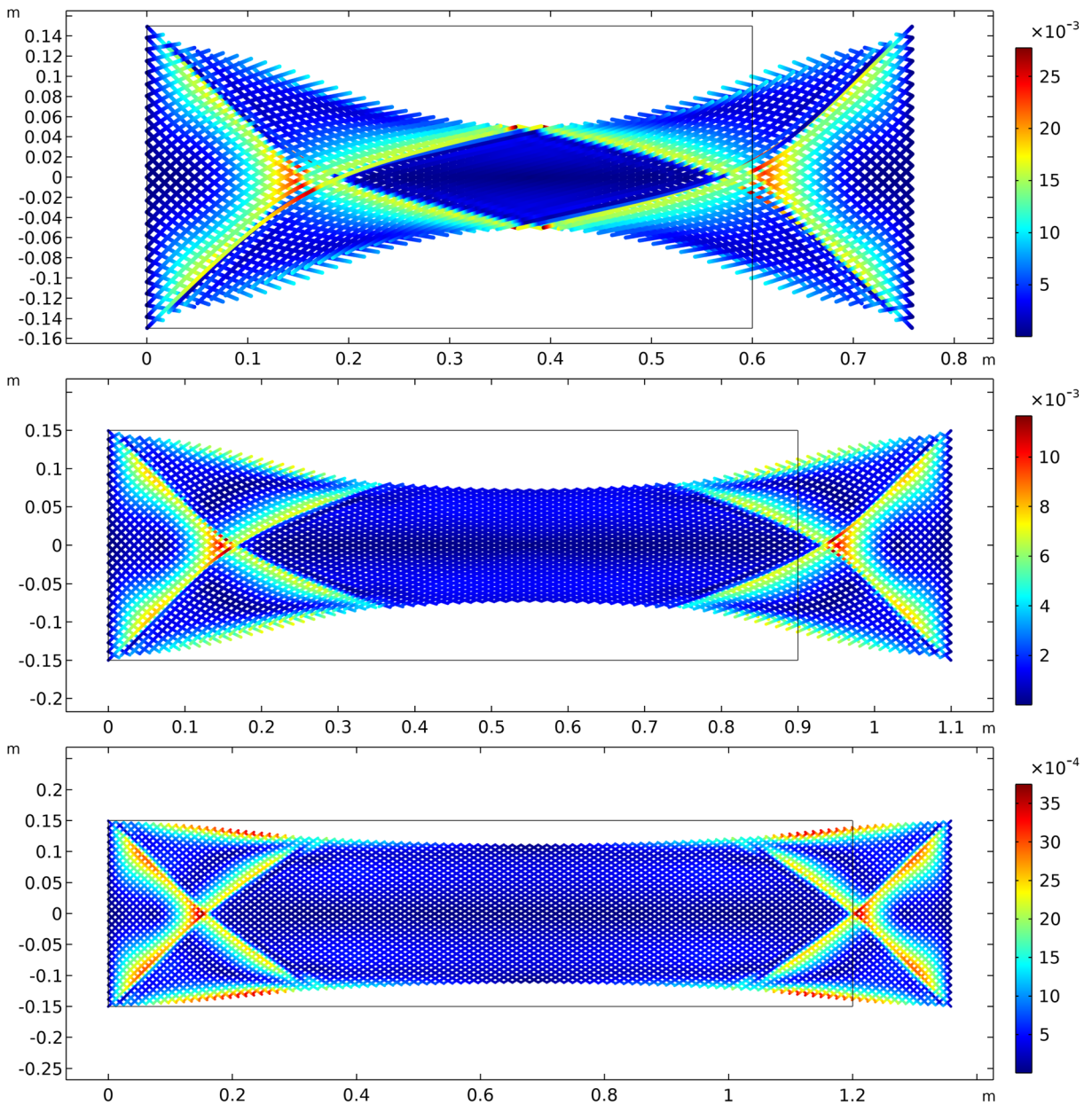
FIG. 8. Relative displacement β for different aspect ratios: 1:2 (top); 1:3 (center); 1:4 (bottom)

3. Numerical results

3.1. Cyclic responses

Numerical simulations based on the energy (2) with dissipation effects due to frictional slip in woven fabrics (9) are performed using a generalized variational principle including Rayleigh dissipative functions
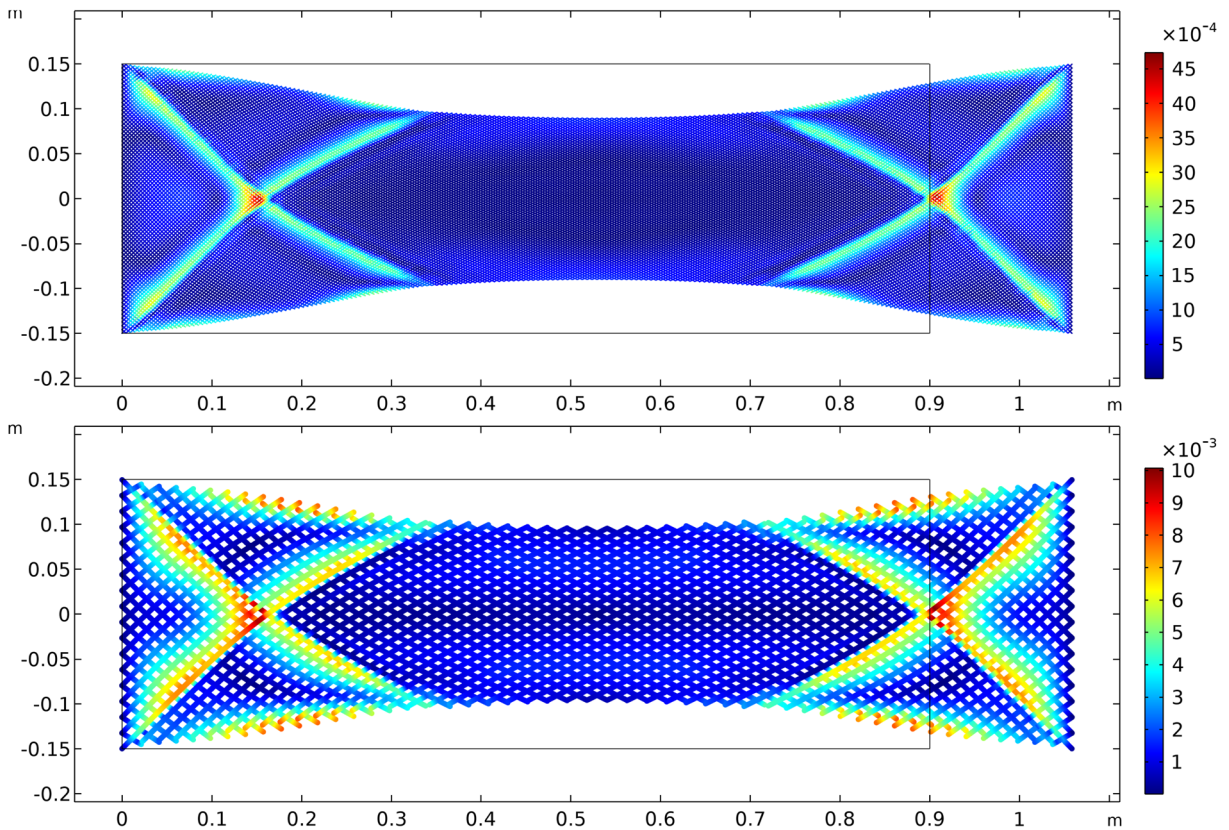
FIG. 9. Comparison between relative displacements for the sample with ratio 1:3 for a soft bending stiffness case (top) and a hard bending stiffness case (bottom)

and the finite element software COMSOL Multiphysics. A nonlinear second gradient energy density characterizes the adopted model. Therefore, particular care is used in the formulation, especially in the right choice of interpolating functions that must be able to represent a functional space H^2 appropriately (see, e.g., [16,53]). To analyze the effect of dissipation in a woven fabric, cyclic tensile tests have been carried out for samples having diverse sizes. Specifically, we considered a rectangular specimen with three aspect ratios, 1:2, 1:3, and 1:4, having a short edge of 30 cm long. The two families of fibers are considered with the same geometry and material. Table 1 reports the parameters used for the simulations unless diversely specified. Identification procedures based on digital image correlation can be used to obtain these parameters experimentally (see, e.g., [27,28,45,46]). We remark that, in the case of dynamic simulations with Coulomb-friction, stick-slip phenomena can occur and need special numerical treatment as given by appropriate integrators [70,71].

We executed these tests by clamping one edge of the sample and applying a given displacement in the longitudinal direction being suppressed the orthogonal component. The cycles are characterized by increasing amplitude even though the maximum velocity in each of them remains the same (see Fig. 2). Here, the idea is to appraise the dissipation for different amplitudes keeping the applied maximal velocity constant to examine the fabric nonlinear response.

Figure 3 shows the force versus displacement plots of the numerical simulations for the different sizes examined under the same imposed displacement. The nonlinear response is more pronounced for the
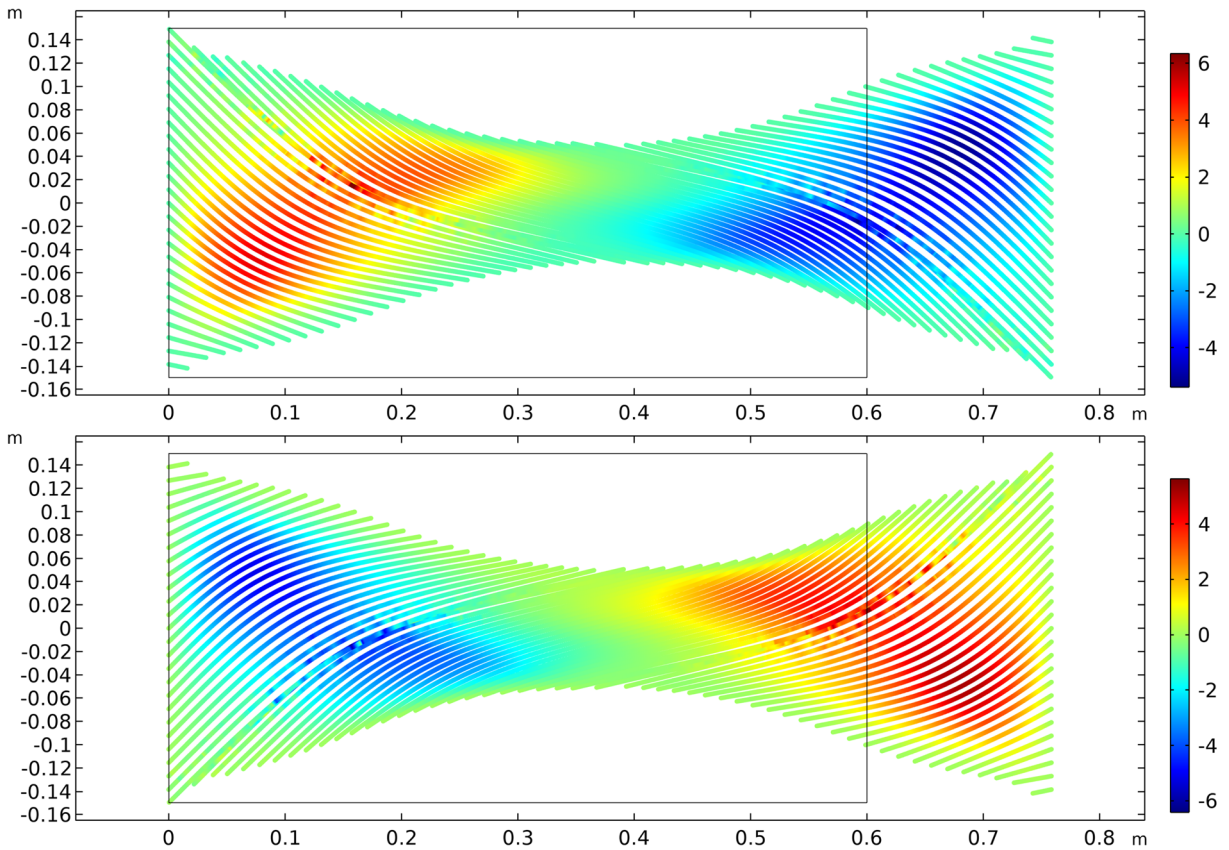
Fig. 10. Curvatures of the sample with the aspect ratio 1:2 under tension: κ_1 (top); κ_2 (bottom)

samples that undergo a large displacement compared with the specimen's overall size. As a matter of fact, for the same displacement, the corresponding value of the force is much larger.

A second test has been conducted with a different axial displacement-controlled loading (see Fig. 4). Instead of keeping the maximal velocity constant, the cycle frequency is set unvarying to see the role of an increasing velocity together with the displacement amplitude. Figure 5 exhibits some differences between the two displacement-controlled loadings because, in the model of dissipation, the regularization of the *signum* function through the hyperbolic tangent implies a certain amount of viscous response that is not provided by the *signum*, which characterizes a pure Coulomb behavior, namely rate-independent. This modeling choice is quite general since, simply changing the slope of the hyperbolic tangent (η), one can vary the share of viscous behavior involved in the motion.

Subsequently, we investigated the role of the stiffnesses on the hysteretic behavior of the fabric. New tensile tests have been carried out with the constant maximal velocity loading in the case of a sample with an aspect ratio of 1:3. In these tests, we considered diminished and increased stiffnesses to illustrate the response of the specimens changing the overall compliance. The stiffnesses used in these tests are: 1) for the soft case $\mathscr{K}_e^\alpha = 8.55 \times 10^7$ N/m and $\mathscr{K}_b^\alpha = 24.05$ N m; 2) for the stiff case $\mathscr{K}_e^\alpha = 1.25 \times 10^8$ N/m and $\mathscr{K}_b^\alpha = 560.8$ N m.

Figure 6 displays the comparison between a significantly soft sample and a stiff one. The former having a more considerable deformation shows a remarkable nonlinear behavior, but the dissipation involved remains low since the internal stress is rather small. The latter, on the contrary, being stiffer,
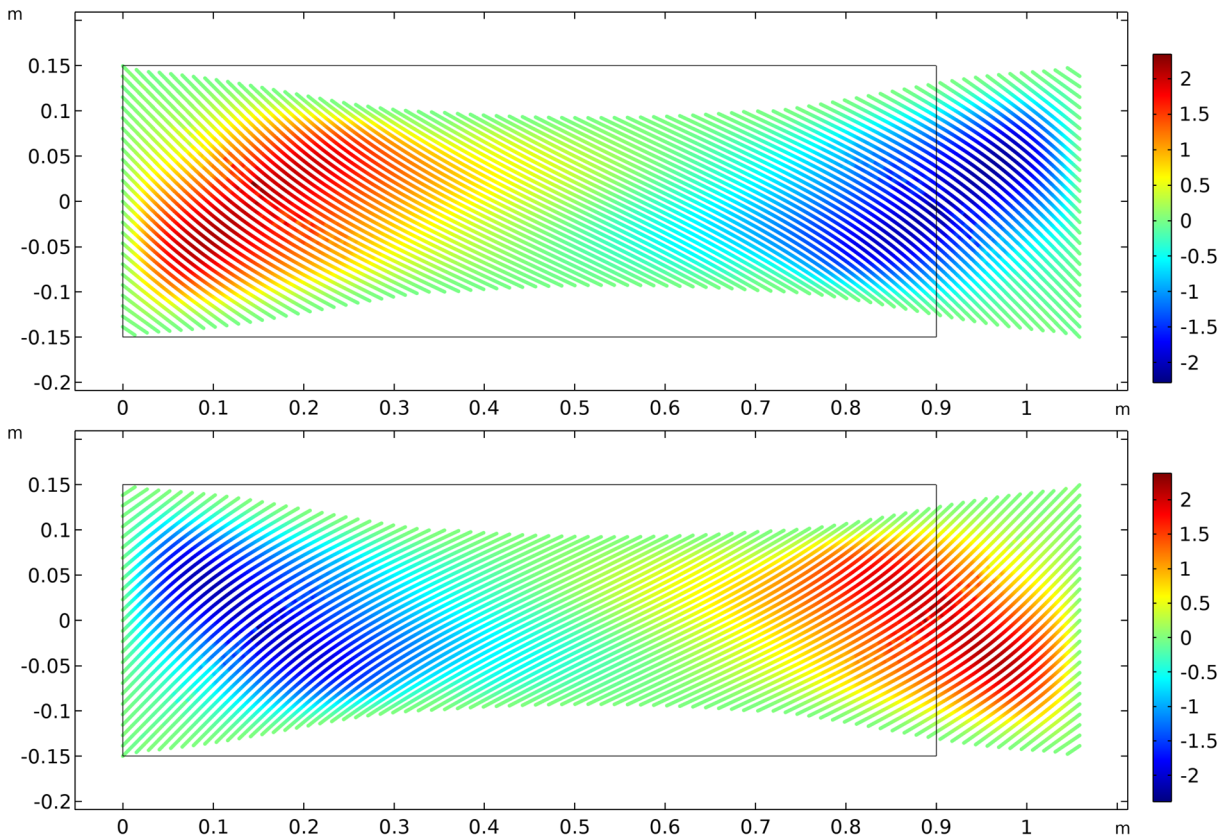
FIG. 11. Curvatures of the sample with the aspect ratio 1:3 under tension: κ_1 (top); κ_2 (bottom)

shows a less pronounced deformation and consequently a more linear response. At the same time, due to a high-stress level, the dissipation is more significant.

Finally, we explored the case in which the previously used model is augmented with the contribution (11) related to the spinning friction. Again, for this case, we compared the two axial displacement-controlled loadings with constant maximal velocity (using the parameters $\zeta_{\text{spin}} = 30$ N/m, $\eta_{\text{spin}} = 40$ s) and constant frequency (using the parameters $\zeta_{\text{spin}} = 80$ N/m, $\eta_{\text{spin}} = 50$ s) for the rectangular sample with an aspect ratio of 1:3. Figure 7 reports the force versus displacement plots. The effect of the spinning friction is evident since the overall dissipation increases compared with the previous cases. The shapes of the hysteretic cycles also change, especially nearby the points of motion reversal. In a detailed description of the dissipative behavior of these materials, one cannot neglect a priori the influence of this phenomenon. Similar comments can be made about the dependence of the imposed displacement history as done before.

3.2. Analysis of the deformation

To have a general picture of the fabric behavior, we showcase the equilibrium shapes of the specimens in the tensile tests in correspondence to the maximum displacement applied. In particular, in what follows, we plot through colors the relative displacement (β), the curvatures of the two families of the fibers (κ_α), and the shear distortion (γ). The first plot is significant to see where the friction phenomenon occurs the most; the second plot represents a quantitative assessment of how meaningful the second-gradient
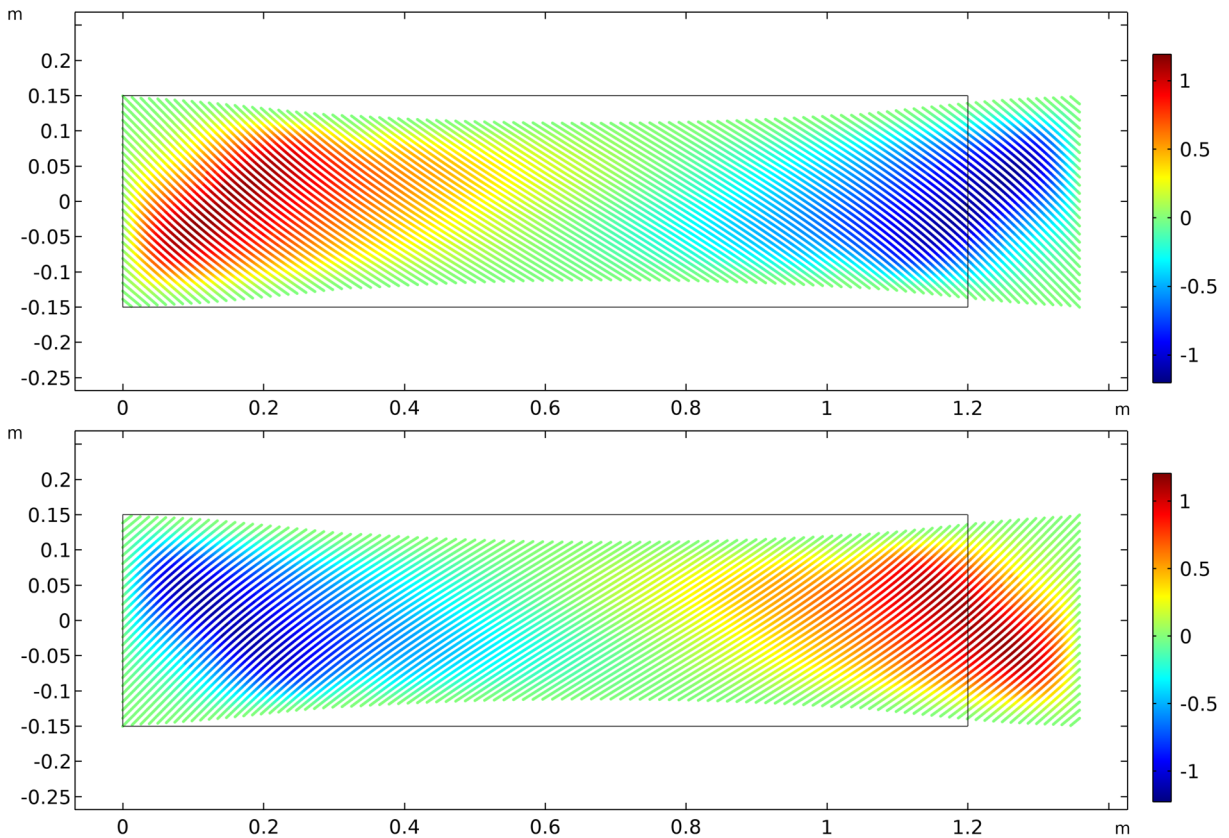
FIG. 12. Curvatures of the sample with the aspect ratio 1:4 under tension: κ_1 (top); κ_2 (bottom)

contribution is; the third is mainly related to the spinning friction. The model used in the numerical simulations is continuous. Still, we display only a few significant material lines in the plots to follow the deformation pattern of the considered samples better. We remark that the finite element discretization is unrelated to the shown lines. On that matter, we set the size of the mesh in order to be sufficiently accurate in obtaining the results, making a convergence analysis.

Figure 8 shows the pattern of the relative displacement involved in the tensile test for different aspect ratios. The qualitative behavior is almost the same, but naturally, the values of the considered field depend on the relative amplitude of the imposed displacement compared with the specimen sizes.

Figure 9 exhibits the effect of the stiffnesses of the fibers. The relative displacement between fibers localizes in the same regions. However, the intensities and the equilibrium shapes of the samples under tension differ.

Figures 10, 11, and 12 show the curvatures of the fibers in the tensile test. The regions for which the curvatures are not vanishing are significant with respect to the overall sizes of the specimen; therefore, the stored energy in the bending deformation cannot be negligible if the related stiffness is sufficiently high. This aspect allows us to assess the importance of the second-gradient contribution in the considered energy.

For the sake of completeness, we also plot the distortion angle γ, which is significant for the definition of the spinning friction, in Fig. 13. This quantity is almost uniform over a large central zone of the sample.
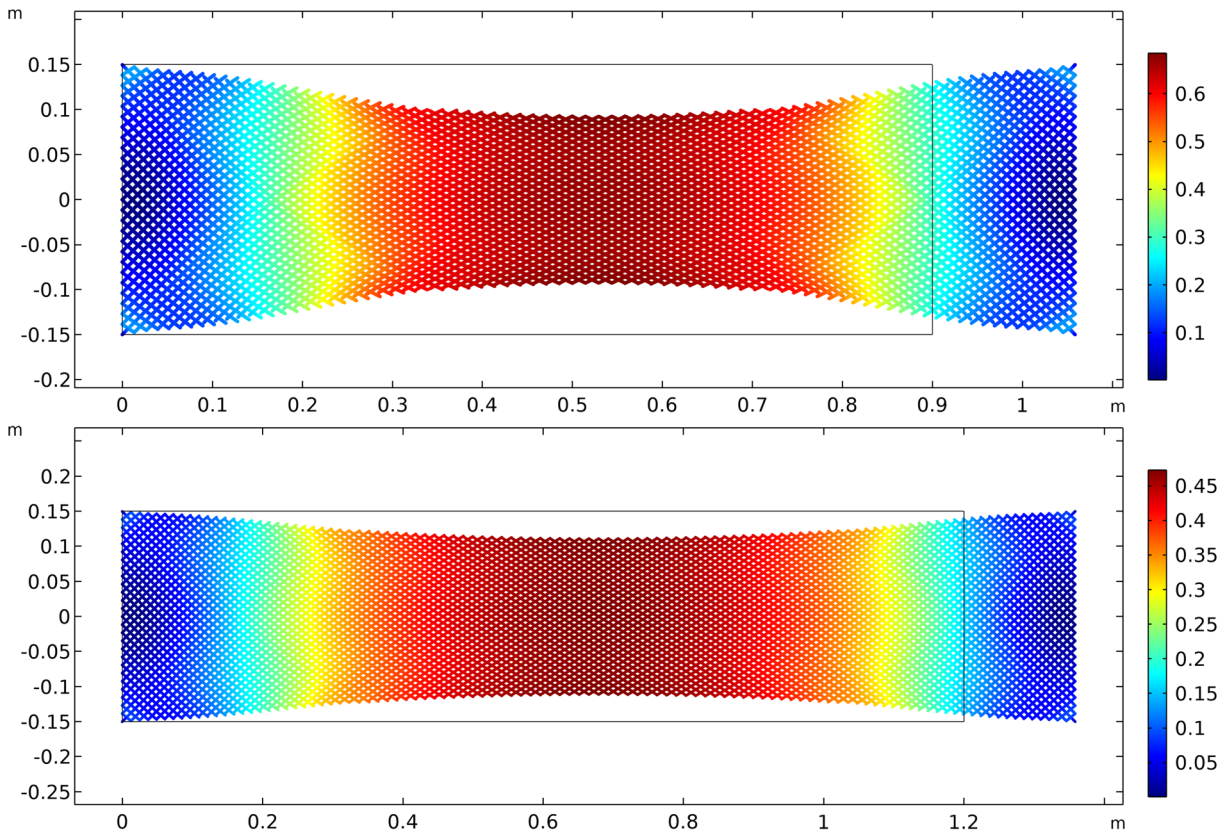
FIG. 13. Distortion angle γ of the sample with the aspect ratio 1:3 (top) and 1:4 (bottom) under tension

4. Conclusions

In the present paper, we propose a weak formulation based on the principle of virtual work to describe the behavior of a planar woven fabric in the framework of continuous deformable surfaces. The model is characterized by an elastic part that takes into account the elongation, and the bending deformations of two orthogonal families of interwoven fibers thought as continuously distributed over a planar reference region. A further contribution in the energy allows us to model the impenetrability of the fibers when they are close to being aligned. The two families of yarns are described by two different independent placement maps, which interact with each other for the effect of the weave but are allowed to possess a relative slipping. This last relative slipping together with the relative rotation between fibers could be a source of dissipation due to friction. In the paper, a suitable Rayleigh functional is introduced to model these phenomena. The effect of the considered friction dissipation is investigated through numerical simulations.

References

[1] Abali, B.E., Barchiesi, E.: Additive manufacturing introduced substructure and computational determination of meta-materials parameters by means of the asymptotic homogenization. Contin. Mech. Thermodyn. **33**(4), 993–1009 (2021)

[2] Abali, B.E., Klunker, A., Barchiesi, E., Placidi, L.: A novel phase-field approach to brittle damage mechanics of gradient metamaterials combining action formalism and history variable. ZAMM-Zeitschrift für Angewandte Mathematik und Mechanik **101**(9), e202000289 (2021)

[3] Alibert, J.J., Seppecher, P., dell'Isola, F.: Truss modular beams with deformation energy depending on higher displace-ment gradients. Math. Mech. Solids **8**(1), 51–73 (2003)

[4] Altenbach, H., Eremeyev, V.A.: On the variational analysis of vibrations of prestressed six-parameter shells. In: Compu-tational Modeling, Optimization and Manufacturing Simulation of Advanced Engineering Materials, pp. 3–19. Springer (2016)

[5] Barchiesi, E., dell'Isola, F., Hild, F.: On the validation of homogenized modeling for bi-pantographic metamaterials via digital image correlation. Int. J. Solids Struct. **208**, 49–62 (2021)

[6] Barchiesi, E., dell'Isola, F., Hild, F., Seppecher, P.: Two-dimensional continua capable of large elastic extension in two independent directions: asymptotic homogenization, numerical simulations and experimental evidence. Mech. Res. Commun. **103**, 103466 (2020)

[7] Barchiesi, E., dell'Isola, F., Laudato, M., Placidi, L., Seppecher, P.: A 1D continuum model for beams with panto-graphic microstructure: asymptotic micro-macro identification and numerical results. In: Advances in Mechanics of Microstructured Media and Structures, pp. 43–74. Springer (2018)

[8] Barchiesi, E., Eugster, S.R., Dell'Isola, F., Hild, F.: Large in-plane elastic deformations of bi-pantographic fabrics: asymptotic homogenization and experimental validation. Math. Mech. Solids **25**(3), 739–767 (2020)

[9] Barchiesi, E., Ganzosch, G., Liebold, C., Placidi, L., Grygoruk, R., Müller, W.H.: Out-of-plane buckling of pantographic fabrics in displacement-controlled shear tests: experimental results and model validation. Contin. Mech. Thermodyn. **31**(1), 33–45 (2019)

[10] Barchiesi, E., Harsch, J., Ganzosch, G., Eugster, S. R.: Discrete versus homogenized continuum modeling in finite deformation bias extension test of bi-pantographic fabrics. Contin. Mech. Thermodyn. 1–14 (2020)

[11] Bersani, A.M., Caressa, P.: Lagrangian descriptions of dissipative systems: a review. Math. Mech. Solids **26**(6), 785–803 (2021)

[12] Bersani, A.M., Caressa, P., dell'Isola, F.: Approximation of dissipative systems by elastic chains: Numerical evidence. Math. Mech. Solids 10812865221081851 (2022)

[13] Boisse, P., Hamila, N., Guzman-Maldonado, E., Madeo, A., Hivet, G., dell'Isola, F.: The bias-extension test for the analysis of in-plane shear properties of textile composite reinforcements and prepregs: a review. Int. J. Mater. Form. **10**(4), 473–492 (2017)

[14] Bolouri, S.E.S., Kim, C.: A model for the second strain gradient continua reinforced with extensible fibers in plane elastostatics. Contin. Mech. Thermodyn. **33**(5), 2141–2165 (2021)

[15] Ciallella, A., Pasquali, D., Gołaszewski, M., D'Annibale, F., Giorgio, I.: A rate-independent internal friction to describe the hysteretic behavior of pantographic structures under cyclic loads. Mech. Res. Commun. **116**, 103761 (2021)

[16] Cordero, N.M., Forest, S., Busso, E.P.: Second strain gradient elasticity of nano-objects. J. Mech. Phys. Solids **97**, 92–124 (2016)

[17] Cuomo, M., dell'Isola, G., Greco, L.: Simplified analysis of a generalized bias test for fabrics with two families of inextensible fibres. Z. Angew. Math. Phys. **67**(3), 1–23 (2016)

[18] dell'Isola, F., Giorgio, I., Pawlikowski, M., Rizzi, N.L.: Large deformations of planar extensible beams and pantographic lattices: heuristic homogenisation, experimental and numerical examples of equilibrium. Proc. Roy. Soc. Lond. A Math. Phys. Eng. Sci. **472**, 2185 (2016)

[19] dell'Isola, F., Lekszycki, T., Pawlikowski, M., Grygoruk, R., Greco, L.: Designing a light fabric metamaterial being highly macroscopically tough under directional extension: first experimental evidence. Z. Angew. Math. Phys. **66**(6), 3473–3498 (2015)

[20] dell'Isola, F., Placidi, L.: Variational principles are a powerful tool also for formulating field theories, volume 535 of Variational Models and Methods in Solid and Fluid Mechanics CISM Courses and Lectures. Springer (2012)

[21] dell'Isola, F., Seppecher, P., Alibert, J.J., et al.: Pantographic metamaterials: an example of mathematically driven design and of its technological challenges. Contin. Mech. Thermodyn. **31**(4), 851–884 (2019)

[22] dell'Isola, F., Seppecher, P., Spagnuolo, M., et al.: Advances in pantographic structures: design, manufacturing, models, experiments and image analyses. Contin. Mech. Thermodyn. **31**(4), 1231–1282 (2019)

[23] Desmorat, B., Spagnuolo, M., Turco, E.: Stiffness optimization in nonlinear pantographic structures. Math. Mech. Solids **25**(12), 2252–2262 (2020)

[24] Eremeyev, V.A., Lebedev, L.P., Cloud, M.J.: The Rayleigh and Courant variational principles in the six-parameter shell theory. Math. Mech. Solids **20**(7), 806–822 (2015)

[25] Eremeyev, V.A., Naumenko, K.: A relationship between effective work of adhesion and peel force for thin hyperelastic films undergoing large deformation. Mech. Res. Commun. **69**, 24–26 (2015)

[26] Eugster, S., dell'Isola, F., Steigmann, D.: Continuum theory for mechanical metamaterials with a cubic lattice substructure. Math. Mech. Complex Syst. **7**(1), 75–98 (2019)

[27] Fedele, R.: Simultaneous assessment of mechanical properties and boundary conditions based on digital image correlation. Exp. Mech. **55**, 139–153 (2015)

[28] Fedele, R., Ciani, A., Galantucci, L., Bettuzzi, M., Andena, L.: A regularized, pyramidal multi-grid approach to global 3D-volume digital image correlation based on X-ray micro-tomography. Fundam. Inf. **125**(3–4), 361–376 (2013)

[29] Ferretti, M., Madeo, A., dell'Isola, F., Boisse, P.: Modeling the onset of shear boundary layers in fibrous composite reinforcements by second-gradient theory. Z. Angew. Math. Phys. **65**(3), 587–612 (2014)

[30] Ganghoffer, J.F., Reda, H.: A variational approach of homogenization of heterogeneous materials towards second gradient continua. Mech. Mater. **158**, 103743 (2021)

[31] Ghafour, T.A., Colmars, J., Boisse, P.: The Dahl's model for the inelastic bending behavior of textile composite preforms. Analysis of its influence in draping simulation. Front. Mater. **8**, 308 (2021)

[32] Ghorbani, A., Dykstra, D., Coulais, C., Bonn, D., van der Linden, E., Habibi, M.: Inverted and programmable Poynting effects in metamaterials. Adv. Sci. **8**(20), 2102279 (2021)

[33] Giorgio, I.: Lattice shells composed of two families of curved Kirchhoff rods: an archetypal example, topology optimization of a cycloidal metamaterial. Contin. Mech. Thermodyn. **33**(4), 1063–1082 (2021)

[34] Giorgio, I., Ciallella, A., Scerrato, D.: A study about the impact of the topological arrangement of fibers on fiber-reinforced composites: some guidelines aiming at the development of new ultra-stiff and ultra-soft metamaterials. Int. J. Solids Struct. **203**, 73–83 (2020)

[35] Giorgio, I., Harrison, P., dell'Isola, F., Alsayednoor, J., Turco, E.: Wrinkling in engineering fabrics: a comparison between two different comprehensive modelling approaches. Proc. Roy. Soc. A Math. Phys. Eng. Sci. **474**(2216), 20180063 (2018)

[36] Giorgio, I., Scerrato, D.: Multi-scale concrete model with rate-dependent internal friction. Eur. J. Environ. Civ. Eng. **21**(7–8), 821–839 (2017)

[37] Giorgio, I., Varano, V., dell'Isola, F., Rizzi, N.L.: Two layers pantographs: a 2D continuum model accounting for the beams' offset and relative rotations as averages in SO (3) Lie groups. Int. J. Solids Struct. **216**, 43–58 (2021)

[38] Greco, L.: An iso-parametric G^1-conforming finite element for the nonlinear analysis of Kirchhoff rod. Part I: the 2D case. Contin. Mech. Thermodyn. **32**(5), 1473–1496 (2020)

[39] Harrison, P.: Modelling the forming mechanics of engineering fabrics using a mutually constrained pantographic beam and membrane mesh. Compos. A Appl. Sci. Manuf. **81**, 145–157 (2016)

[40] Harrison, P., Clifford, M.J., Long, A.C.: Shear characterisation of viscous woven textile composites: a comparison between picture frame and bias extension experiments. Compos. Sci. Technol. **64**(10), 1453–1465 (2004)

[41] La Valle, G.: A new deformation measure for the nonlinear micropolar continuum. Z. Angew. Math. Phys. **73**(2), 1–26 (2022)

[42] Massoumi, S., La Valle, G.: Static analysis of 2D micropolar model for describing granular media by considering relative rotations. Mech. Res. Commun. **119**, 103812 (2022)

[43] Nadler, B., Steigmann, D.J.: A model for frictional slip in woven fabrics. C.R. Mech. **331**(12), 797–804 (2003)

[44] Nase, M., Rennert, M., Naumenko, K., Eremeyev, V.A.: Identifying traction-separation behavior of self-adhesive polymeric films from in situ digital images under T-peeling. J. Mech. Phys. Solids **91**, 40–55 (2016)

[45] Nejadsadeghi, N., De Angelo, M., Misra, A., Hild, F.: Multiscalar DIC analyses of granular string under stretch reveal non-standard deformation mechanisms. Int. J. Solids Struct. 111402 (2022)

[46] Nejadsadeghi, N., Hild, F., Misra, A.: Parametric experimentation to evaluate chiral bars representative of granular motif. Int. J. Mech. Sci. **221**, 107184 (2022)

[47] Placidi, L.: A variational approach for a nonlinear one-dimensional damage-elasto-plastic second-gradient continuum model. Contin. Mech. Thermodyn. **28**(1), 119–137 (2016)

[48] Placidi, L., Barchiesi, E., Misra, A.: A strain gradient variational approach to damage: a comparison with damage gradient models and numerical results. Math. Mech. Complex Syst. **6**(2), 77–100 (2018)

[49] Placidi, L., Greco, L., Bucci, S., Turco, E., Rizzi, N.L.: A second gradient formulation for a 2D fabric sheet with inextensible fibres. Z. Angew. Math. Phys. **67**(5), 114 (2016)

[50] Reda, H., Karathanasopoulos, N., Elnady, K., Ganghoffer, J.-F., Lakiss, H.: The role of anisotropy on the static and wave propagation characteristics of two-dimensional architectured materials under finite strains. Mater. Des. **147**, 134–145 (2018)

[51] Reda, H., Karathanasopoulos, N., Rahali, Y., Ganghoffer, J.-F., Lakiss, H.: Influence of first to second gradient coupling energy terms on the wave propagation of three-dimensional non-centrosymmetric architectured materials. Int. J. Eng. Sci. **128**, 151–164 (2018)

[52] Scerrato, D., Giorgio, I., Madeo, A., Limam, A., Darve, F.: A simple non-linear model for internal friction in modified concrete. Int. J. Eng. Sci. **80**, 136–152 (2014)

[53] Scerrato, D., Zhurba Eremeeva, I.A., Lekszycki, T., Rizzi, N.L.: On the effect of shear stiffness on the plane deformation of linear second gradient pantographic sheets. ZAMM-Zeitschrift für Angewandte Mathematik und Mechanik **96**(11), 1268–1279 (2016)

[54] Sessa, S., Vaiana, N., Paradiso, M., Rosati, L.: An inverse identification strategy for the mechanical parameters of a phenomenological hysteretic constitutive model. Mech. Syst. Signal Process. **139**, 106622 (2020)

[55] Shekarchizadeh, N., Abali, B.E., Barchiesi, E., Bersani, A.M.: Inverse analysis of metamaterials and parameter determination by means of an automatized optimization problem. ZAMM-Zeitschrift für Angewandte Mathematik und Mechanik **101**(8), e202000277 (2021)

[56] Spagnuolo, M., Barcz, K., Pfaff, A., dell'Isola, F., Franciosi, P.: Qualitative pivot damage analysis in aluminum printed pantographic sheets: numerics and experiments. Mech. Res. Commun. **83**, 47–52 (2017)

[57] Spagnuolo, M., Franciosi, P., dell'Isola, F.: A Green operator-based elastic modeling for two-phase pantographic-inspired bi-continuous materials. Int. J. Solids Struct. **188**, 282–308 (2020)

[58] Spagnuolo, M., Yildizdag, M. E., Pinelli, X., Cazzani, A., Hild, F.: Out-of-plane deformation reduction via inelastic hinges in fibrous metamaterials and simplified damage approach. Math. Mech. Solids 10812865211052670

[59] Stilz, M., Plappert, D., Gutmann, F., Hiermaier, S.: A 3D extension of pantographic geometries to obtain metamaterial with semi-auxetic properties. Math. Mech. Solids 10812865211033322 (2021)

[60] Tornabene, F., Viscoti, M., Dimitri, R.: Equivalent single layer higher order theory based on a weak formulation for the dynamic analysis of anisotropic doubly-curved shells with arbitrary geometry and variable thickness. Thin-Walled Struct. **174**, 109119 (2022)

[61] Turco, E.: A numerical survey of nonlinear dynamical responses of discrete pantographic beams. Contin. Mech. Thermodyn. **33**(4), 1465–1485 (2021)

[62] Turco, E., Barchiesi, E.: Equilibrium paths of Hencky pantographic beams in a three-point bending problem. Math. Mech. Complex Syst. **7**(4), 287–310 (2019)

[63] Turco, E., Barchiesi, E., dell'Isola, F.: A numerical investigation on impulse-induced nonlinear longitudinal waves in pantographic beams. Math. Mech. Solids **27**(1), 22–48 (2022)

[64] Vaiana, N., Sessa, S., Rosati, L.: A generalized class of uniaxial rate-independent models for simulating asymmetric mechanical hysteresis phenomena. Mech. Syst. Signal Process. **146**, 106984 (2021)

[65] Vangelatos, Z., Melissinaki, V., Farsari, M., Komvopoulos, K., Grigoropoulos, C.: Intertwined microlattices greatly enhance the performance of mechanical metamaterials. Math. Mech. Solids **24**(8), 2636–2648 (2019)

[66] Wang, C., Vangelatos, Z., Winston, T., Sun, S., Grigoropoulos, C. P., Ma, Z.: Remodeling of architected mesenchymal microtissues generated on mechanical metamaterials. 3D Print. Addit. Manuf. (2021)

[67] Yang, H., Abali, B.E., Timofeev, D., Müller, W.H.: Determination of metamaterial parameters by means of a homogenization approach based on asymptotic analysis. Contin. Mech. Thermodyn. **32**(5), 1251–1270 (2020)

[68] Yildizdag, M.E., Barchiesi, E., dell'Isola, F.: Three-point bending test of pantographic blocks: numerical and experimental investigation. Math. Mech. Solids **25**(10), 1965–1978 (2020)

[69] Sailer, S., Eugster, S.R., Leine, R.I.: The Tippedisk: a Tippetop Without Rotational Symmetry. Regul. Chaot. Dyn. **25**(6), 553–580 (2020). https://doi.org/10.1134/S1560354720060052

[70] Capobianco, G., Harsch, J., Eugster, S.R., Leine, R.I.: A nonsmooth generalized-alpha method for mechanical systems with frictional contact. Int. J. Numer. Methods Eng. **122**(22), 6497–6526 (2021). https://doi.org/10.1002/nme.6801

[71] Capobianco, G., Eugster, S.R.: Time finite element based Moreau-type integrators. Int. J. Numer. Methods Eng. **114**(3), 215–231 (2018). https://doi.org/10.1002/nme.5741

Alessandro Ciallella and Ivan Giorgio
DICEAA - Department of Civil, Construction-Architectural and Environmental Engineering
University of L'Aquila
L'Aquila
Italy
e-mail: ivan.giorgio@univaq.it

Alessandro Ciallella
e-mail: alessandro.ciallella@univaq.it

Daria Scerrato
SBAI - Department of Basic and Applied Sciences for Engineering
University of Rome La Sapienza
Rome
Italy
e-mail: daria.scerrato@uniroma1.it

Mario Spagnuolo
DICAAR - Department of Environmental Civil Engineering and Architecture
University of Cagliari
Cagliari
Italy
e-mail: mario.spagnuolo@unica.it